International Environmental Modelling and Software Society (iEMSs)
2010 International Congress on Environmental Modelling and Software
Modelling for Environment's Sake, Fifth Biennial Meeting, Ottawa, Canada
David A. Swayne, Wanhong Yang, A. A. Voinov, A. Rizzoli, T. Filatova (Eds.)
http://www.iemss.org/iemss2010/index.php?n=Main.Proceedings

Experimental study of the critical criteria for incipient sediment movement using a simple model eddy

R J Munro [a]

[a]*Environmental Fluid Mechanics Group, Process and Environmental Research Division, Faculty of Engineering, University of Nottingham, Nottingham NG7 2RD, UK (rick.munro@nottingham.ac.uk)*

Abstract: Experiments have been performed to study the interaction between a sediment layer and a vortex ring (used, here, as an idealised model for an isolated turbulent eddy). Attention was focussed on studying the interaction under "critical" conditions, in which motion of sediment grains was only just induced by the flow field of the vortex ring. Near-spherical monodisperse sediment grains were used throughout with relative density 2.5 and diameters (d_p) ranging between 0.053 mm and 1.0 mm. Measurements of the vortex-ring flow field were obtained, during the period of interaction, using two-dimensional particle imaging velocimetry (PIV). The conditions for incipient sediment motion were investigated in terms of the critical Shields parameter (θ_c), defined in terms of the peak tangential velocity measured directly above the bed surface and obtained from the PIV data. Effects due to increases in bed slope were studied by tilting the sediment bed at various angles between the horizontal and the repose angle for sediment. The measured values of θ_c are compared and discussed in terms of the particle Reynolds number (based on the particle settling velocity and d_p), the ratio d_p/δ (where δ is the viscous sublayer thickness), and the bed slope.

Keywords: Sediment transport and erosion, Shields parameter, vortex ring, turbulent eddy.

1 INTRODUCTION

Sediment transport is associated with high Reynolds number flows and turbulence. Many of the widely used sediment transport models characterise the flow turbulence by averaged quantities, such as the mean bed shear stress or mean flow rate (White [1940], Francis [1973]). The motion and entrainment of sediments, however, are not driven by these average characteristics, but by the fluctuating forces exerted by the flow on the near-surface grains (Schmeeckle et al. [2007]). Consequently, the average quantities of the flow can only parameterise the underlying physical processes that cause sediment erosion, and so standard models often provide inconsistent and inaccurate predictions (Nelson et al. [1995]). Therefore, clarification of the complex and intermittent turbulence-sediment interaction is essential to improve our understanding of the sediment erosion and transport processes, and to increase the accuracy of predictive models.

It is broadly recognised that coherent vortex structures (within a turbulent flow) that interact with, or originate within, the near-bed region are a key mechanism controlling the movement, entrainment and transport of sediments (Yung et al. [1989]; Rashidi et al. [1990]; Kaftori et al. [1995]; Niño and Garcia [1996]). The vortex ring represents one of the simplest (coherent) vortex structures, which can be easily and consistently produced in the laboratory. Moreover, the vortex ring has been used with considerable success in a number of previous studies as an idealised model for a turbulent entrainment (Maxworthy [1972]) and, in particular, as a model for turbulent entrain-

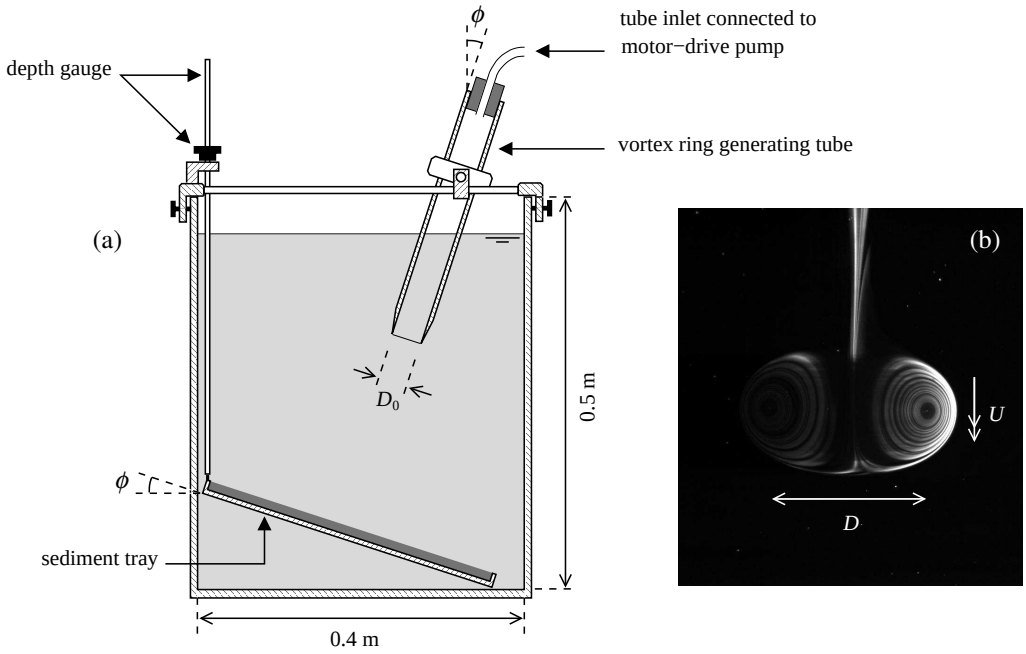

Figure 1: (a) Sketch of the experiment apparatus. (b) Cross-section through a fully developed vortex ring, illustrating how the ring diameter (D) is defined and the direction and speed (U) of propagation. The ring shown has diameter $D = 48$ mm and Reynolds number $Re = \rho UD/\nu = 3400$.

ment mechanism across a sharp density interface (Linden [1973]; Dahm et al. [1989]). Furthermore, recent work by Munro et al. [2009] investigated how a sediment layer is eroded by the flow field of a vortex ring interacting with the layer surface. Several non-intrusive, camera-based techniques were used to measure small-scale erosion levels in the sediment layer (Munro and Dalziel [2005]; Munro et al. [2004]) over a broad range of conditions, both during and after the interaction. The experiments described here further extend this work to investigate the critical conditions under which the flow field of the interacting vortex ring is sufficient to only just induce motion of the near surface sediment grains. These critical conditions for incipient sediment motion are studied for various sediment sizes and also as a function of bed slope (between the horizontal and up to the repose limit). The details of the experiments are provided in Section 2, with results and summary given in Sections 3 and 4.

2 EXPERIMENTS

A sketch of the basic apparatus is shown in Figure 1(a). The experiments were performed in a rectangular acrylic tank containing water. A range of monodisperse near-spherical sediments were used with grain diameters (d_p) ranging between 0.053-1.0 mm and with relative density $\gamma = \rho_p/\rho = 2.5$ (where ρ_p and ρ denote sediment and fluid densities respectively). Each sediment layer was formed on a flat, shallow tray, with the surface of the layer made smooth by carefully drawing a flat scraper across the top rim of the tray. This produced a close-packed bed of mean depth 5 mm. The properties of each sediment type are summarised in Table 1, where w_s denotes the settling velocity of a single grain and $Re_p = \rho w_s d_p/\mu$ is the particle Reynolds number (where μ denotes the fluid dynamic viscosity).

Each vortex ring was generated using a motor-driven pump mechanism (which is described in detail by Munro et al. [2009]) connected, via an air-tight seal, to a cylindrical tube (of internal diameter $D_0 = 0.04$ m and length 0.4 m), with the tube outlet partially submerged below the water free-surface (see Figure 1a). Hence, as the motor actuates the pump the air-filled cavity within the tube expands, forcing a predetermined volume of water from the tube outlet. The vortex sheet

Label	$\gamma = \rho_p/\rho$	d_p (mm)	w_s (mm/s)	Re_p	ϕ_r (deg)
A	2.5	0.053	9.1	0.5	23
B	2.5	0.20	31.0	6.2	25
C	2.5	0.70	92.1	64.4	27
D	2.5	1.00	151.5	151.5	28

Table 1: Basic properties of the sediment particles.

shed at the lip of the outlet, as the fluid exits the tube, roles up and forms a vortex ring (Maxworthy [1972]; Saffman [1975]). Once fully formed the vortex ring propagates away from the outlet along the symmetry axis of the tube, until impacting on the sediment layer surface at the base of the tank. Moreover, each vortex ring travelled a relatively short distance (approximately $5D_0 = 0.2\,\mathrm{m}$) before the ring structure and trajectory were affected by the presence of the sediment layer. Over this short distance the ring diameter, D, and propagation speed, U, were found to be near constant. Figure 1(b) shows an image of a cross-section through a fully developed vortex ring illustrating how the ring diameter D is defined (*i.e.*, the diameter of the vortex core). The motor-driven actuation system was calibrated so that the propagation speed U, diameter D and hence Reynolds number $Re = \rho UD/\mu$ of each vortex ring could be pre-determined as a function of the actuation rate of the pump. A detailed description of this calibration procedure is given in Munro et al. [2009] and Munro and Dalziel [2005]. For the range of experiments considered here, Re was varied between 600 and 3400, with D/D_0 in the range 0.9 to 1.2.

Effects due to variations in bed slope were analysed by tilting the sediment tray at various angles ϕ at the start of a given experiment (as shown in see Figure 1a). The corresponding bed slope is defined as $\beta = \tan\phi$. For each sediment type, experiments were performed at bed angles in the range $\phi \in [0, \phi_r)$, where ϕ_r denotes the measured repose angle for the sediment. The mechanism used to the tilt the tray consisted of simple depth gauge attached to one side of the tray which could be wound up (or down) to set the required angle (see Figure 1a). To prevent the sediment layer sliding on the smooth tray surface when tilted, the tray base was roughened by gluing a thin layer of sediment particles to its surface. The repose angle, ϕ_r, for each sediment type was measured by carefully increasing the bed angle from $\phi = 0$ until the bedform became unstable and collapsed. The corresponding values of ϕ_r obtained using this procedure are shown in Table 1. In each experiment attention was focussed on interactions in which the central propagation axis of the vortex ring was perpendicular to the sediment bed surface. Hence, the tube used to generate each vortex ring was held within an adjustable clamp that could tilt the tube at the corresponding angle ϕ to the vertical, as shown in Figure 1(a).

The critical conditions for incipient sediment motion were determined by repeating an experiment for a given sediment type, each time decreasing Re (by decreasing U) until grain motion was only just observed to occur, with any further decrease in Re resulting in no motion. During this procedure the sediment layer was re-scraped and made flat prior to repeating each experiment. Once the critical conditions had been identified for a given sediment type (and for a given bed slope β), the flow field of the (axisymmetric) vortex ring during the interaction period was measured using two-dimensional particle imaging velocimetry (PIV). For each PIV experiment, small neutrally-buoyant tracer particles were used to seed the water volume, with the mid-plane of the vortex trajectory illuminated by a narrow, vertical light sheet. The trajectories of the seeding particles were recorded using a high-speed digital camera (sampling at 500-600 Hz), positioned to view through the tank sidewall. The velocity fields were calculated using PIV techniques found in Digiflow. For the angled-bed cases ($\phi > 0$) the camera was tilted on its side at the corresponding angle ϕ, and aligned so that the surface of the sediment layer appeared horizontal at the base of each image. Fluid velocity data, under critical conditions for incipient grain motion, was obtained for each sediment type, and at various bed slopes. A typical vortex-ring velocity field obtained using PIV is shown in Figure 2(a), where z denotes distance normal to and above the bed, and x denotes tangential distance across the bed surface.

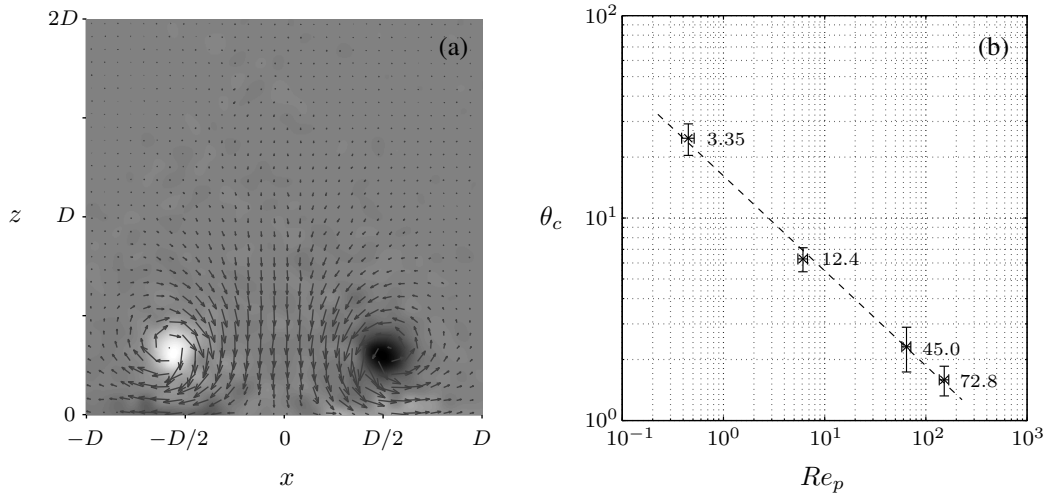

Figure 2: (a) Typical PIV measurements obtained through the midplane of a vortex ring (with $D = 48$ mm and $Re = 3400$) interacting with a sediment layer of type D. (b) Measured values of θ_c plotted against Re_p for each sediment type, for the flat bed case ($\beta = 0$). Also shown (next to each data point) are the corresponding values of d_p/δ. Error bars are included, calculated using estimates for rms variations in $u_{0,c}$ and w_s. The broken line shows the fitted curve $\theta_c = k_1 Re_p^{-n}$, with $k_1 = 16.2$, $n = 0.469$.

3 RESULTS

Sediment transport is commonly described in terms of the dimensionless Shields parameter, which in the present context can be defined as

$$\theta = \frac{\tau}{(\gamma - 1)\rho d_p g \cos\phi}, \tag{1}$$

where τ denotes the bed shear stress. The Shields parameter may be interpreted as the ratio of the hydrodynamic drag force, $\mathcal{O}(\tau d_p^2)$, exerted by the flow, which acts on the exposed surface area of a sediment grain, and the component of the grain weight, $\mathcal{O}((\gamma-1)\rho d_p^3 g \cos\phi)$, normal to the bed surface (*viz.*, the normal reaction force). Forces due to cohesion are known to only be significant for fine sediments, typically with $d_p \lesssim 0.03$ mm (Phillips [1980]), and so here we expect drag and buoyancy to be the dominant terms in the force balance for sediment motion.

For each sediment type there will exist a critical value of bed shear stress, denoted τ_c, at and above which motion of sediment grains is induced, and below which the sediment remains stationary. The experiments described here were performed under critical conditions, although the bed shear stress (τ_c) was not measured. Note that, in the case of steady turbulent channel flow, estimation of τ_c is standard (*e.g.*, White [1970] uses $\tau_c = \rho g H \beta$, where H is the channel depth and β the bed slope). However, in the experiments described here the boundary layer induced by the interacting vortex ring evolves spatially and with time, and the mean velocity profile within this region is not known. Hence, a standard estimation of τ_c using an analogous procedure was not possible. However, Munro et al. [2009] showed that when a vortex ring interacts with a sediment layer the tangential fluid velocity immediately above the bed surface attains a maximum value directly below the cores of the ring. Moreover, it was shown that the onset of sediment motion consistently occurs directly below this region of peak tangential flow, with the displaced sediment grains moving along, predominantly, radial trajectories away from the ring centre (as illustrated by Figures 7 and 8 in Munro et al. [2009]). Hence, the bed shear stress, τ, will scale with ρu_0^2, where u_0 denotes the peak tangential velocity close the sediment surface, during the period of interaction, which here was taken to be the maximum attained value of the tangential flow at a height $z = 1$ mm above the bed surface. (This is as close to the bed surface at which reliable and consistent velocity measurements could be obtained with the setup described.) Using this estimate

the critical Shields parameter, denoted θ_c, can be defined as

$$\theta_c = \frac{u_{0,c}^2}{(\gamma - 1) d_p g \cos\phi}, \tag{2}$$

where $u_{0,c}$ denotes the value of u_0 obtained under critical conditions for incipient sediment motion.

Note that, under critical conditions (and ignoring bed permeability effects) we expect the depth of the boundary layer induced by the vortex ring above the bed surface to be $\mathcal{O}(DRe^{-1/2})$ and the thickness of the inner viscous sublayer, denoted δ, to be $\mathcal{O}(DRe^{-1})$ (Munro et al. [2009]). Therefore, the magnitude of the drag force acting on the near-surface sediment grains will be dependent on d_p/δ. That is, if the grain size is large in comparison with the sublayer thickness, the vertical velocity gradient acting across the grain will scale with the outer inviscid flow immediately above the boundary layer region (*i.e.*, $u_{0,c}$). In this case, the drag force induced on the grain by the flow will be $\mathcal{O}(\rho u_{0,c}^2 d_p^2)$. However, if $d_p/\delta \lesssim \mathcal{O}(1)$ viscous stresses act to reduce both the fluid velocity and velocity gradient acting on and across the grain, and so the drag force acting on the grain is reduced and is $\mathcal{O}(\rho u_{0,c}^4 d_p^4/\nu^2)$ (Munro et al. [2009]). To initiate grain motion, therefore, the induced drag force must overcome the frictional force λN, where λ is the contact friction coefficient and $N = \pi(\gamma - 1)\rho d_p^3 g \cos\phi/6$ is the normal reaction force acting on the grain. When d_p is large compared δ, equating the drag and friction forces gives the condition that $\theta_c \sim \mathcal{O}(1)$ and constant (for constant λ), whereas for $d_p/\delta \leqslant 1$ the corresponding condition gives $\theta_c \sim Re_p^{-1/2}$ (Eames and Dalziel [2000]).

The measured values of θ_c for each sediment type are shown in Figure 2(b), plotted against particle Reynolds number, Re_p. The data shown are for the flat bed case only (*i.e.*, $\beta = 0$ or $\phi = 0$). Also shown in Figure 2(b) are the corresponding values of d_p/δ (next to each data point) and the curve $\theta_c = k_1 Re_p^{-n}$ (shown as the broken line), where the values $k_1 = 16.2$ and $n = 0.469$ have been fitted (by least squares) to the data points. The fit suggests that the data shown in Figure 2(b) are consistent with the $\theta_c \sim Re_p^{-1/2}$ scaling, corresponding to the $d_p/\delta \sim \mathcal{O}(1)$ and $Re_p \ll 1$ limiting case. It is worth noting, however, that the data presented in the previous studies of both Eames and Dalziel [2000] and Munro et al. [2009] (albeit, data for the critical conditions for sediment resuspension, not sediment movement) showed that the transition between the $\theta_c \sim Re_p^{-1/2}$ scaling and the $\theta_c \sim \mathcal{O}(1)$ regime occurred at $Re_p \approx 1$ with $d_p/\delta \approx 15$. Hence, it can be argued that the data for the largest two values of d_p/δ in Figure 2(b) are, in fact, consistent with the $\theta_c \sim \mathcal{O}(1)$ (and constant) regime; that is, for $d_p/\delta = 45.0$ and 72.8, the corresponding values of θ_c are near constant with $\theta_c \approx 2$. Additional analysis is required here, using a broader range of sediment types and sizes, to further investigate the transition between these two regimes.

The effects due to variations in bed slope are shown in Figure 3(a). Noting that, as the bed slope (β) increases towards the repose limit the critical shear stress (τ_c) is expected to decrease towards zero. That is, the sediment layer becomes unstable at the repose limit, with grain motion induced (due to the component of grain weight acting down the slope) in the absence of any shear stress imposed by fluid motion. It follows, therefore, that $\theta_c \to 0$ as $\beta/\beta_r \to 1$ (where $\beta_r = \tan\phi_r$ the bed slope at the repose angle). Hence, to facilitate this comparison the measured values of θ_c shown in Figure 3(a) are plotted against $(1 - \beta/\beta_r)$, with each of the four symbols representing a different sediment type (see caption for details). The data shown in Figure 3(a) confirm the expected monotonic decrease in θ_c towards zero as $\beta/\beta_r \to 1$, with the data for each sediment type being well described by the power-law relationship of the form

$$\theta_c = k_2 \left(1 - \frac{\beta}{\beta_r}\right)^m. \tag{3}$$

In the above equation, the parameters k_2 and m are functions of the particle type (*i.e.*, functions of particle Reynolds number, Re_p). The broken lines included in Figure 3(a) show the results of fitting equation (3) separately to each of the four data sets (by the least squares method). Noting that when $\beta = 0$ (*i.e.*, when the sediment layer is flat with $\phi = 0$), it follows immediately that $k_2 \equiv k_1 Re_p^{-n}$, where $k_1 = 16.2$ and $n = 0.469$ are simply the fitted values obtained for the

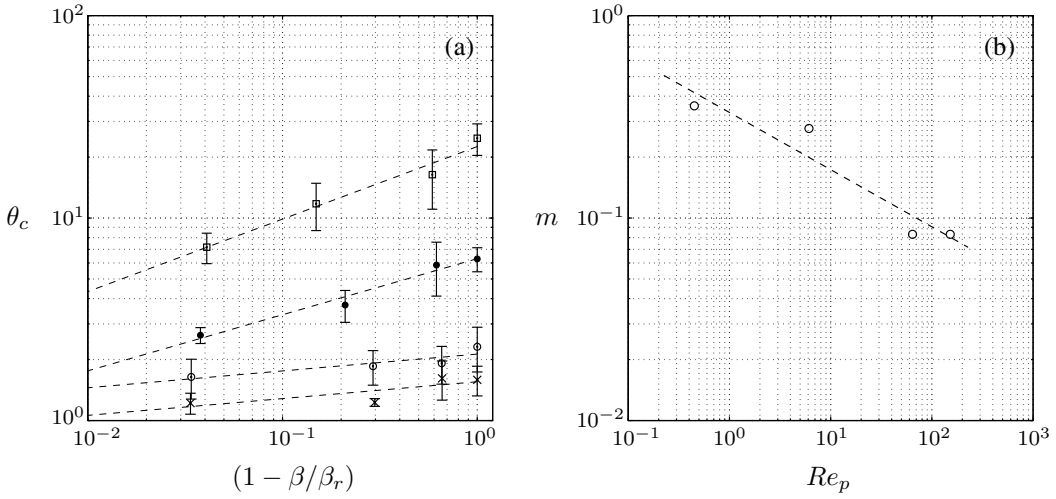

Figure 3: (a) Measured values of θ_c plotted against $(1-\beta/\beta_r)$ (where $\beta_r = \tan\phi_r$ is the bed slope at the repose limit). The symbols □, •, ○ and × correspond to sediment types A, B, C and D respectively. Also shown (broken lines) are the corresponding curves $\theta_c = k(1-\beta/\beta_r)^m$, fitted to each data set using least squares. The error bars shown are based on rms variations in the measured values of $u_{0,c}$. (b) The fitted values of m plotted against particle Reynolds number Re_p. The broken line shows the fitted curve, $m = k_3 Re_p^{-q}$, with $k_3 = 0.332$ and $q = 0.282$.

flat bed case shown in Figure 2(b). Moreover, the data in Figure 3(a) show that at each fixed bed slope, β, there is a clear monotonic decrease in θ_c with increasing Re_p. Hence, it follows that the exponent m in equation (3) is expected to decrease monotonically with increasing Re_p. This is confirmed in Figure 3(b) which shows the corresponding fitted values of the exponent m plotted against Re_p. Also shown (by the broken line) is the curve $m = k_3 Re_P^{-q}$, where the fitted values $k_3 = 0.332$ and $q = 0.282$ were obtained using least squares.

4 SUMMARY AND FINAL REMARKS

The experiments presented here were used to investigate the critical conditions for the onset of grain motion induced by an isolated vortex ring interacting with a sediment layer. A selection of near-spherical sediments were used, with grain diameters ranging between 0.053 mm and 1.0 mm and with a relative density of 2.5. The effects due to variations in bed slope were considered, between zero slope and up to the repose limit. In all cases each vortex ring was aligned to approach the layer from a direction normal to the layer surface, in an otherwise quiescent fluid. The critical conditions for grain movement were analysed in terms of the critical Shields parameter, $\theta_c = u_{0,c}^2/(\gamma-1)d_p g\cos\phi$, defined in terms of the peak tangential flow measured above the sediment layer surface. In particular, θ_c was examined as a function of particle Reynolds number, Re_p, dimensionless particle size, d_p/δ (where δ is the characteristic viscous sublayer thickness), and the bed slope, β.

The data suggest (see Figure 2b) that for the finer sediment types (with $Re_p \lesssim 10$, $d_p/\delta \lesssim 13$) viscous stresses act to significantly reduce the hydrodynamic drag forces induced on the near-surface sediment grains, resulting in a monotonic increase in θ_c with decreasing Re_p (and decreasing d_p/δ); in this range the data were also found to be consistent with the $\theta_c \sim Re_p^{-\frac{1}{2}}$ scaling which corresponds to the $Re_p \ll 1$ limit. For the larger sediment types (with $Re_p \gtrsim 60$, $d_p/\delta \gtrsim 40$) the measured values of θ_c are near constant with $\theta_c \approx 2$, which is consistent with the case $\theta_c \sim \mathcal{O}(1)$ (and constant) corresponding to when d_p is large in comparison with δ. It is also worth noting that the above observations are consistent with the "hydrodynamic roughness" limit (*i.e.*, $d_p = 0.2$ mm) proposed by White [1970].

The variations in θ_c caused by increases in bed slope were analysed by comparing the measured

values of θ_c in terms of $(1 - \beta/\beta_r)$ (see Figure 3a). The data confirmed the expected behaviour that $\theta_c \to 0$ in the limit as $\beta/\beta_r \to 1$, with the measured values of θ_c for each sediment type considered being well described by the power law relationship given in equation (3). The monotonic decrease in the exponent m (see Figure 3b) with increasing Re_p consistent with the observed monotonic decrease in θ_c with increasing Re_p found (and expected) for the particle types (and sizes) considered here.

The process of sediment transport is complex and poorly understood, with current models (based on simple parameterisations using mean flow quantities) being unreliable and often inconsistent. To improve such models, we need to account for the intermittent, fluctuating hydrodynamic forces that give rise to sediment motion and entrainment, forces which are typically associated with the most energetic eddies within the flow. Although the experiments presented here are not directly applicable to fully established turbulent flows, they are intended as an idealised description (or model) of a typical intermittent turbulent "burst", and the results provide insight into how an isolated turbulent structure (or coherent eddy), interacting with a sediment layer, gives rise to grain motion. Experiments to extend this work are currently ongoing to investigate the correlation between the vortex flow field (during the interaction period) and the corresponding induced velocities of the near-surface sediment grains. Moreover, future experiments are planned to apply a similar analysis to investigate sediment movement and entrainment induced by zero-mean stationary turbulence generated using an oscillating grid.

ACKNOWLEDGMENTS

This work was supported by the Engineering and Physical Sciences Research Council (EPSRC grant number EP/H007032/1). The author gratefully acknowledges Ben Cooper-Smith, Damien Goy, Mike Langford, Hanna Mohtar and Tom Shaw for technical support.

REFERENCES

Dahm, W. J. A., C. M. Scheil, and G. Tryggvason. Dynamics of a vortex ring interacting with a density interface. *Journal of Fluid Mechanics*, 205:1–43, 1989.

Eames, I. and S. B. Dalziel. Dust resuspension by the flow around an impacting sphere. *Journal of Fluid Mechanics*, 403:305–328, 2000.

Francis, J. R. D. Experiments on the motion of solitary grains along the bed of a water-stream. *Proceedings of the Royal Socieity of London Series A*, 332:443–465, 1973.

Kaftori, D., G. Hetsroni, and S. Banerjee. Particle behaviour in the turbulent boundary layer. 1. motion, deposition and entrainment. *Physics of Fluids*, 7:1095–1106, 1995.

Linden, P. F. The interaction of a vortex ring with a sharp density interface: a model for turbulent entrainment. *Journal of Fluid Mechanics*, 60:467–480, 1973.

Maxworthy, T. The structure and stability of vortex rings. *Journal of Fluid Mechanics*, 51:15–32, 1972.

Munro, R. J., N. Bethke, and S. B. Dalziel. Sediment resuspension and erosion by vortex rings. *Physics of Fluids*, 21:046601, 2009.

Munro, R. J. and S. B. Dalziel. Attenuation technique for measuring sediment displacement levels. *Experiments in Fluids*, 39:600–611, 2005.

Munro, R. J., S. B. Dalziel, and H. Jehan. A pattern matching technique for measuring sediment displacement levels. *Experiments in Fluids*, 37:399–408, 2004.

Nelson, J. M., R. L. Shreve, S. R. McLean, and T. G. Drake. Role of near-bed turbulence structure in bed load transport and bed form mechanics. *Water Resources Research*, 31:2071–2086, 1995.

Niño, Y. and M. H. Garcia. Experiments on particle-turbulence interactions in the near-wall region of an open channel flow: implications for sediment transport. *Journal of Fluid Mechanics*, 326: 285–319, 1996.

Phillips, M. A force balance model for particle entrainment into a fluid stream. *Journal of Physics D–Applied Physics*, 13:221–233, 1980.

Rashidi, M., G. Hetsroni, and S. Banerjee. Particle-turbulence interaction in a boundary layer. *International Journal of Multiphase Flow*, 16:935–949, 1990.

Saffman, P. G. On the formation of vortex rings. *Studies in Applied Mathematics*, 54:371–380, 1975.

Schmeeckle, M. W., J. M. Nelson, and R. L. Shreve. Forces on stationary particles in near-bed turbulent flows. *Journal of Geophysical Research*, 112:F02003, 2007.

White, C. M. The equilibrium of grains in the bed of a stream. *Proceedings of the Royal Socieity of London Series A*, 174:322–338, 1940.

White, S. J. Plane bed thresholds for fine grained sediments. *Nature*, 228:152–155, 1970.

Yung, B. P. K., H. Merry, and T. R. Bott. The role of turbulent bursts in particle re-entrainment in aqueous systems. *Chemical Engineering Science*, 44:873–882, 1989.